An Improved SPICE Model of SiC BJT Incorporating Surface Recombination Effect

Jun Wang, *Senior Member, IEEE*, Shiwei Liang, *Student Member, IEEE*, Linfeng Deng, Xin Yin, and Z. John Shen, *Fellow, IEEE*

***Abstract*—The SiC bipolar junction transistor (BJT) offers an attractive alternative to the more popular SiC MOSFET. It is important to develop an accurate SPICE model for the SiC BJT to enable its use in power electronic applications. The current gain of an SiC BJT may degrade considerably at high current levels and/or at high temperatures largely due to the surface recombination effect. In this paper, an improved SPICE behavioral model that accurately accounts for the current gain depending on the collector current and the junction temperature is proposed for the SiC BJT. In this paper, the conventional Gummel–Poon model is extended to include this important physical effect by adding a diode between the external base and emitter terminals of the BJT. A two-step model parameter extraction method is developed. First, the basic Gummel–Poon model parameters are extracted from low-current measurement data, and then, the new surface recombination model parameters are extracted by observing the difference between the measured high-level base current and the standard Gummel–Poon model prediction. The simulated static and switching characteristics of the new SiC BJT model match the measured data very well. Finally, the new SPICE model is used in the performance assessment of a proportional base driver technique embedded in a 3.6-kW boost converter, demonstrating its validity in helping with the optimum design of power electronic applications based on SiC BJTs.**

***Index Terms*—Bipolar junction transistor (BJT), proportional base driver, SPICE model, surface recombination effect, 4H-SiC.**

I. Introduction

WHILE the SiC power MOSFET is the most popular high-voltage wide bandgap semiconductor device today, the SiC bipolar junction transistor (BJT) is still an attractive alternative for high power density and/or high-temperature power conversion applications because of its several unique advantages, such as lower specific ON-resistance, simpler fabrication process, and free from oxide reliability concerns under high electrical field and at high temperatures. Although it has the drawback of a relatively large base consumption because of its

Manuscript received May 4, 2018; revised July 19, 2018; accepted September 4, 2018. Date of publication September 19, 2018; date of current version May 2, 2019. This work was supported in part by the National Natural Science Foundation of China under Grant 51577054 and in part by the Science and Technology Major Project of Hunan Province under Grant 2017GK1020. Recommended for publication by Associate Editor D. Costinett. *(Corresponding authors: Shiwei Liang and Linfeng Deng.)*

The authors are with the College of Electrical and Information Engineering, Hunan University, Changsha 410082, China (e-mail:

-

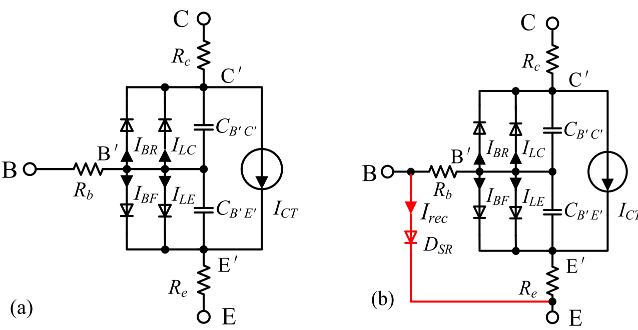

Fig. 1. Schematics of (a) Gummel–Poon model and (b) proposed SRGP model.

nomena were ignored. Johannesson and Nawaz [17] developed an analytical PSPICE model for SiC BJT power modules based on the Gummel–Poon model, which is helpful for the design of power electronic applications based on SiC BJT power modules. Mantooth *et al*. [18] established a physical-based model for the SiC BJT by iteratively fitting the characteristics of the SiC BJT on MATLAB/Simulink platform. However, the model does not take into account the temperature effect and is insufficiently accurate to predict the current gain of the SiC BJT at different temperatures.

The purpose of this paper is to propose a simple semi-physical model for the SiC BJT that is capable of accurately predicting its current gain over a wide range of collector current and operation temperatures. To achieve this objective, we extend the conventional Gummel–Poon model to a novel surface recombination Gummel–Poon (SRGP) model incorporating the surface recombination effect. In Section II, the conventional Gummel–Poon model is introduced, and its extension to the SRGP model is illustrated. Section III presents the extraction process of modeling parameters. In Section IV, static and dynamic performances of the SRGP model at different collector currents and elevated temperatures are verified, and its implementation in a discrete 1200-V/10-A SiC BJT based 3.6-kW 200-kHz power converter for the performance assessment of a proportional base driver is presented. Finally, the conclusion is given in Section V.

II. Gummel–Poon Model Extension

A. Gummel–Poon Model

The widely used Gummel–Poon model is utilized as the fundamental model, and its schematic is shown in Fig. 1(a). The Gummel–Poon model consists of a current source and four diodes, which are used to represent specific physical parameters, such as the collector current $I_{\rm CT}$, the forward base current $I_{\rm BF}$, the reverse base current $I_{\rm BR}$, the emitter leakage current $I_{\rm LE}$, and the collector leakage current $I_{\rm LC}$. A detailed analytical description of the Gummel–Poon model is presented in the following [16]:

$$I_{\rm BF} = \frac{I_S}{\beta_F}\left(\exp\left(\frac{qV_{B'E'}}{N_F kT}\right) - 1\right) \tag{1}$$

$$I_{\rm BR} = \frac{I_S}{\beta_R}\left(\exp\left(\frac{qV_{B'C'}}{N_R kT}\right) - 1\right) \tag{2}$$

$$I_{\rm LE} = I_{\rm SE}\left(\exp\left(\frac{qV_{B'E'}}{N_E kT}\right) - 1\right) \tag{3}$$

$$I_{\rm LC} = I_{\rm SC}\left(\exp\left(\frac{qV_{B'C'}}{N_C kT}\right) - 1\right) \tag{4}$$

$$I_{\rm CT} = I_S\left(\exp\left(\frac{qV_{B'E'}}{N_F kT}\right) - \exp\left(\frac{qV_{B'C'}}{N_R kT}\right)\right) \tag{5}$$

where I_S is the transport saturation current, N_F is the forward current emission coefficient, $V_{B'E}$ is the internal terminal voltage between the base and emitter terminals, β_F is the ideal maximum forward current gain, $V_{B'C'}$ is the internal terminal voltage between base and collector terminals, N_R is the reverse current emission coefficient, β_R is the ideal maximum reverse current gain, $I_{\rm SE}$ is the base and emitter leakage saturation current, N_E is the base and emitter leakage emission coefficient, $I_{\rm SC}$ is the base and collector leakage saturation current, N_C is the base and collector leakage emission coefficient, *k* is the Boltzmann's constant, *q* is the elementary charge, and *T* is the temperature.

Its dynamic performance is mainly determined by the internal capacitances, built up by the SCRs in the p/n junctions. The capacitances are modeled under forward bias and reverse bias conditions [16], [17], respectively. However, a discontinuous behavior of capacitances may occur at zero bias, inducing convergence troubles. Therefore, the capacitances under forward and reverse conditions are modeled as follows:

$$C_{\rm BE} = \frac{C_{\rm JE}}{(1 - V/V_{\rm JE})^{\rm MJE}} \tag{6}$$

$$C_{\rm BC} = \frac{C_{\rm JC}}{(1 - V/V_{\rm JC})^{\rm MJC}} \tag{7}$$

where $C_{\rm JE}$ is the depletion capacitance when zero bias is applied between base and emitter terminals, $C_{\rm JC}$ is the depletion capacitance when zero bias is applied between the base and collector terminals, $V_{\rm JE}$ and $V_{\rm JC}$ are the built-in potentials of emitter and collector junctions, respectively, and MJE and MJC are the exponential factors of the emitter and collector junctions, respectively.

The temperature dependence of the SPICE model strongly affects the accuracy in predicting the SiC BJT's performance at elevated temperatures. In the Gummel–Poon model, the temperature dependence is correlated with a set of parameters, including the transport saturation current I_S, the ideal maximum forward current gain β_F, the ideal maximum reverse current gain β_R, the base and emitter leakage saturation current $I_{\rm SE}$, and the base and collector leakage saturation current $I_{\rm SC}$. All these parameters are extended with temperature coefficients and written as follows [19]:

$$I_S\,(T) = I_S\,(T_0)\left(\frac{T}{T_0}\right)^{\rm XTI}\exp\left[\frac{E_g}{V_T}\left(\frac{T}{T_0} - 1\right)\right] \tag{8}$$

$$\beta(T) = \beta(T_0)\left(\frac{T}{T_0}\right)^{\mathrm{XTB}} \tag{9}$$

$$I_{\mathrm{SE}}(T) = I_{\mathrm{SE}}(T_0)\left(\frac{T}{T_0}\right)^{-\mathrm{XTB}}\left(\frac{I_S(T)}{I_S(T_0)}\right)^{1/N_E} \tag{10}$$

$$I_{\mathrm{SC}}(T) = I_{\mathrm{SC}}(T_0)\left(\frac{T}{T_0}\right)^{-\mathrm{XTB}}\left(\frac{I_S(T)}{I_S(T_0)}\right)^{1/N_C}. \tag{11}$$

To solve (8), we use two physics-related auxiliary variables given by [17]

$$V_T = \frac{kT}{q} \tag{12}$$

$$E_g = 3.263 - \frac{6.5\times10^{-4}\cdot T^2}{T\,+\,1300} \tag{13}$$

where XTI is the temperature exponent for the effect on I_S, E_g is the bandgap of 4H-SiC, XTB is the forward and reverse beta temperature coefficient, and V_T is the thermal potential.

The quasi-saturation region between the forward active region and the saturation region in the output characteristics of the SiC BJT is modeled with a voltage-dependent collector resistance [16]. The same collector resistance equation is used, and one of the scale functions is replaced by the physics-based temperature-dependent intrinsic carrier concentration. The voltage-dependent collector resistance R_C accounting for the quasi-saturation effects is expressed as follows:

$$R_C = \frac{R_{C0}}{\frac{1}{2}+\frac{1}{4}\sqrt{1+\frac{4n_i^2}{N_{\mathrm{epi}}^2}\exp\left(\frac{qV_{B'C'}}{kT}\right)}+\frac{1}{4}\sqrt{1+\frac{4n_i^2}{N_{\mathrm{epi}}^2}\exp\left(\frac{qV_{B'C}}{kT}\right)}} \tag{14}$$

where n_i is the intrinsic carrier concentration, N_{epi} is the epilayer collector doping concentration, which is 4.8×10^{15} cm^{-3} in the model, and $V_{B'C'}$ and $V_{B'C}$ are voltages at each end of the collector resistance. The zero-bias collector resistance R_{C0} is determined by

$$R_{C0} = 2.143\times10^{-21}\cdot\exp(0.1302\cdot T). \tag{15}$$

B. Surface Recombination Gummel–Poon Model (SRGP)

Since the surface recombination effect is not considered in the Gummel–Poon model, it is insufficiently accurate to predict the current gain of the SiC BJT at large collector currents and/or high temperatures. To solve this problem, we extend the conventional Gummel–Poon model by considering the surface recombination effect in this paper. Based on Shockley–Read–Hall (SRH) recombination theory, we model this important physical effect by adding a diode between the external base and emitter terminals of the BJT to the Gummel–Poon model, as shown in Fig. 1(b).

A typical half-cell cross-sectional structure of a 1200-V SiC BJT is shown in Fig. 2(a). Generally, there are four recombination mechanisms in a SiC BJT [7], [8], including the recombination in the neutral bulk of base and emitter regions and SCRs in

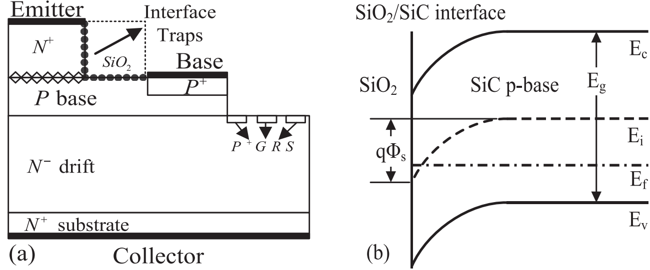

Fig. 2. (a) Schematic cross-sectional structure of the SiC BJT [21]. (b) Energy band diagram of the SiC/SiO_2 interface.

the emitter junction and at the SiC/SiO_2 interfaces. Unlike the high quality of Si/SiO_2 interface in the Si BJT, there are high density interface traps at the SiC/SiO_2 interfaces in the SiC BJT [20]. These interface traps act as recombination centers, causing the pinning effect on the Fermi level. Hence, the band diagram near the SiC/SiO_2 interface is bended, as shown in Fig. 2(b). At the interface, electrons are accumulated and injected into the base region, forming a stable surface recombination current on the surface [7].

The surface recombination effect occurring at the SiC/SiO_2 interface can be explained by the SRH recombination theory. The dependence of the surface recombination rate on the hole and electron densities is described by the following expression [22]:

$$R_{\mathrm{SRH}} = \frac{n_s p_s - n_i^2}{(n_s+n_1)/s_p + (p_s+p_1)/s_n} \tag{16}$$

with

$$n_1 = n_i\exp\left(\frac{E_{\mathrm{trap}}}{kT}\right) \tag{17}$$

and

$$p_1 = n_i\exp\left(\frac{-E_{\mathrm{trap}}}{kT}\right) \tag{18}$$

where n_i is the intrinsic carrier concentration, n_s and p_s are electron and hole densities at the depleted surface, respectively, n_1 is the balanced electron density in the conduction band when the electron Fermi level is at the trap level, p_1 is the balanced hole density in the value band when the hole Fermi level is at the trap level, and s_n and s_p are the electron and hole recombination velocities, respectively. The term n_i^2 is equal to $n_1 p_1$ and is usually smaller than the product of electron density n_s and hole density p_s, when the bias voltage is larger than several times of *kT*/*q*. The product of electron density n_s and hole density p_s is expressed as follows:

$$n_s p_s = n_i^2\exp\left(qV_{B'E'}/kT\right). \tag{19}$$

Typically, the doping concentration of the base region of a SiC BJT is smaller than 1e18 cm^3 to obtain a large current gain; hence, it is treated as a non-degenerate semiconductor when analyzing its band diagram. The electron density is extremely small compared with the total state density in the conduction band because of rapid electron emission, and the hole density is quite small compared with the total state density in the valence

band because of rapid hole emission [23]. Its conduction band is almost empty, while the valence band is almost fully occupied. Therefore, the terms n_1 and p_1 can be ignored because the electron and hole emissions are negligible compared with the captures. Equation (16) can be simplified as follows:

$$R_{\mathrm{SRH}} = \frac{(s_n s_p n_s p_s)^{1/2}}{\lambda^{1/2} + \lambda^{-1/2}} \tag{20}$$

with

$$\lambda = \frac{s_n n_s}{s_p p_s}. \tag{21}$$

The surface recombination current density is equal to the electron charge multiplying the integration of the surface recombination rate over the depletion width *x* and is given by

$$J_{\mathrm{rec}} = q \int R_{\mathrm{SRH}} dx. \tag{22}$$

Substituting (17)–(19) into (20) yields

$$J_{\mathrm{rec}} = \frac{q(s_n s_p)^{1/2} n_i W}{2\left(\lambda^{1/2} + \lambda^{-1/2}\right)} \exp\left(\frac{qV_{B'E'}}{2kT}\right) \tag{23}$$

where *W* is assumed to be the width of the depletion region at the interface.

Since the base region is treated as a non-degenerate semiconductor, the surface state induced deep levels should be neither empty nor fully occupied in order to make the surface remain neutral with the varying charge in the depletion layer, when a large bias is applied. This requires the ratio of n_s and p_s to be almost a constant, which means almost a constant λ [23]. Therefore, as given in (21), the surface recombination current density shows an exponential growth with the bias voltage between the internal base and emitter terminals, which is similar to a diode's forward *I–V* characteristic, and an ideality factor of approximately 2 is suggested if a diode D_{SR} is used to model the surface recombination effect. Since the surface condition may vary, the emission coefficient of the diode modeled for the surface recombination effect is found to be in the range of 1.5–4 in [24]. However, the diode describing the forward base current behavior of the SiC BJT has an ideality factor of approximately 1, which cannot effectively describe the sum of the surface recombination current and the forward base current. Although the diode describing the base and emitter leakage currents has an ideality factor of approximately 2, it is difficult to have the same ideality factor as that of the surface recombination current and to effectively model the leakage current simultaneously. Therefore, an additional diode D_{SR} between the external base and emitter terminals of the BJT is proposed to extend the conventional Gummel–Poon model and include the surface recombination effect in this paper, as shown in Fig. 1(b).

The relationship between the surface recombination current and base–emitter forward bias voltage in the additional diode D_{SR} is expressed as follows:

$$I_{\mathrm{rec}} = I_{\mathrm{SR}} \left(\exp\left(\frac{q\left(V_{\mathrm{BE}} - I_{\mathrm{rec}} R_S\right)}{N_{\mathrm{SR}} kT}\right) - 1\right) \tag{24}$$

with

$$I_{\mathrm{SR}} = \frac{q(s_n s_p)^{1/2} n_i W A}{2\left(\lambda^{1/2} + \lambda^{-1/2}\right)} \tag{25}$$

where I_{SR} is defined as the additional diode's saturation current, R_S is the series resistance, N_{SR} is the additional diode's emission coefficient, V_{BE} is the bias voltage applied on the diode, and *A* is the area of periphery of the emitter fingers of an SiC BJT.

The temperature dependence of the additional diode's saturation current is given by

$$I_{\mathrm{SR}}(T) = I_{\mathrm{SR}}(T_0) \left(\frac{T}{T_0}\right)^{\frac{\mathrm{XTI_{Dsr}}}{N_{\mathrm{SR}}}} \exp\left[\frac{E_g}{V_T}\left(\frac{T}{T_0} - 1\right)\right] \tag{26}$$

where $\mathrm{XTI}_{D\mathrm{sr}}$ is the temperature coefficient of the additional diode's saturation current.

III. Model Parameters Extraction

A 1200-V/10-A SiC BJT (GA10JT12-247) from GeneSiC is characterized and modeled in this paper. It has an n^+-p^--n^--n^+ layer structure, as shown in Fig. 2(a) [21]. To develop the SRGP model, we establish a two-step method to extract the model parameters. We first extract the Gummel–Poon model parameters under small base current condition where the surface recombination effect can be neglected and, then, extract the surface recombination model parameters by observing the difference between the measured high-level base current and the standard Gummel–Poon model prediction.

The dc characteristics of the SiC BJT were measured with the power device analyzer Agilent B1505A. The pulse mode was utilized so that the self-heating effect could be reduced during the measurement process. The dynamic characteristics were measured using a double pulse test (DPT) setup under inductive load conditions. The measured characteristics were, then, used for the extraction of modeling parameters and validation of the model. The experimental details of measurements are given in [25]. To extract the modeling parameters of the fundamental Gummel–Poon model, the characteristics of the SiC BJT were measured with a relatively small current first. Then, the measured *I–V* characteristics along with the base–emitter and base–collector diode characteristics at different temperatures were fitted using (1)–(5) and (8)–(11). Using (1)–(5) to fit the measured *I–V* characteristics at room temperature, the SiC BJT's SPICE modeling parameters, such as the transport saturation current parameter I_S, the forward and reverse current gains β_F, β_R, and the ideality factors N_F, N_R, N_E, N_C, were extracted. The temperature dependence of the Gummel–Poon model is based on a set of parameters, such as the transport saturation current and the ideal maximum forward current gain, which is represented by the scale functions. The temperature coefficients XTI and XTB were extracted by fitting the temperature-dependent characteristics using (8) and (9). In addition, the measured *C–V* characteristics have little sensitivity to the operation temperatures [25]; hence, the temperature coefficients of the internal capacitances of the SiC BJT are ignored. The modeling parameters were, thereafter, manually fine-tuned with iterations of

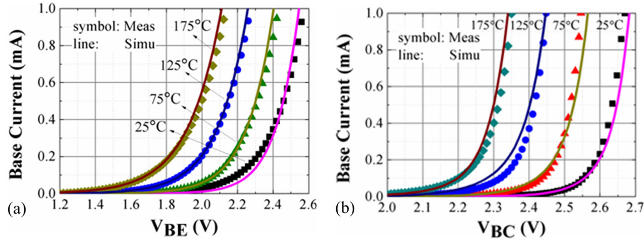

Fig. 3. Forward *I–V* diode characteristics of (a) emitter junction and (b) collector junction.

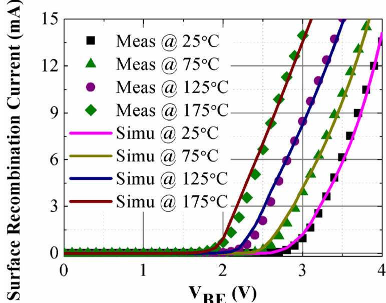

Fig. 4. Extraction of the surface recombination current.

small changes to optimize the SiC BJT's characteristics at small currents. The measured and SPICE-simulated base–emitter and base–collector diode characteristics at different temperatures are shown in Fig. 3.

The surface recombination current induced by the SiC/SiO_2 interface traps is part of the total base current, and it cannot be measured directly. Since the developed standard Gummel–Poon model can be regarded as an ideal description of the SiC BJT without surface recombination, the SPICE-simulated base current with the developed standard Gummel–Poon model is treated as the ideal base current without surface recombination, while the measured base current includes the contribution from the surface recombination current. We observe the difference between the measured high-level base current and the standard Gummel–Poon model prediction from the output characteristic simulations $(I_C - V_{\text{CE}})$ at the same relatively large collector–emitter voltage and collector current and treat it as the surface recombination current. The extracted surface recombination current is expressed as follows:

$$I_{\text{rec}} = I_{Bm} - I_{Bs} \tag{27}$$

where I_{rec} is the surface recombination current, I_{Bm} is the measured base current, and I_{Bs} is the predicted base current simulated by the developed standard Gummel–Poon model at the same collector–emitter voltage and collector current as the measurements.

Fig. 4 shows the variation of the extracted surface recombination current with the base–emitter voltage at different temperatures. The surface recombination current shows an exponential growth with the base–emitter voltage and has a positive temperature coefficient. The positive temperature coefficient is mainly induced by the dependence of the carrier concentration and the surface potential barrier height on temperature. When the ambient temperature increases, the intrinsic carrier concentration increases, and the turn-ON knee voltage of the p/n junction reduces. Moreover, the increased thermal energy also enhances surface trapping and recombination process by facilitating the migration of more generated unpaired electrons toward the surface. Therefore, the surface recombination rate is increased by the enhancement of free carrier trapping rate on the surface. The model parameters of the additional diode in the SRGP model were extracted by fitting the surface recombination current at different base–emitter voltages and temperatures using (22) and (24). The extracted emission coefficient of the diode is 3.05 and the series resistance is 31.7 Ω. A good match between the fitting curves and the extracted surface recombination current at various base–emitter voltages and temperatures was obtained, as shown in Fig. 4.

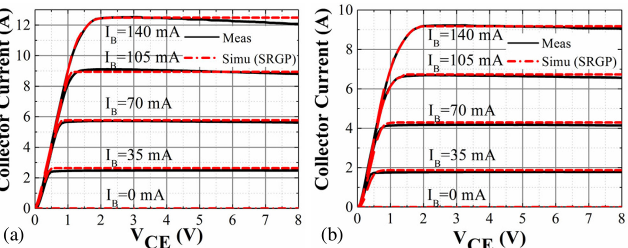

Fig. 5. Measured and SPICE-simulated output characteristics of the SiC BJT. (a) At room temperature. (b) At 150 °C.

IV. Model Validation and Implementation

A. Model Validation

The SRGP model can be constructed as a subcircuit and implemented in a SPICE simulator. To demonstrate the effectiveness of the SRGP model, the static and dynamic characteristics of the SiC BJT were measured and compared with the SPICE simulation results under different conditions. The simulated and experimental output characteristics at various base currents (35, 70, 105, and 140 mA) at room temperature and at 150 °C are shown in Fig. 5. The simulation results of the SRGP model show satisfactory agreement with these experimental data at various base currents and temperatures. It is observed that an increasing collector voltage leads to a decrease of the collector current, when the collector current is higher than 6 A in the active region. This is induced by the self-heating effect, although the pulse mode with an appropriate pulsewidth and period was selected to suppress the self-heating effect in the measurement of the SiC BJT's output characteristics. Owing to the relatively strong self-heating effect at a large collector current, the junction temperature of the SiC BJT increases during the measurement, inducing the reduction of current gain and collector current.

To verify the validity of the SRGP model over a wide current and temperature range, we compared the SPICE-simulated and measured forward current gains at different collector currents and temperatures. Fig. 6 shows the SPICE-simulated and measured current gains versus the collector current at $V_{\text{CE}} = 5$ V and at room temperature. It is found that the SPICE-simulated current gain of the SiC BJT using the conventional

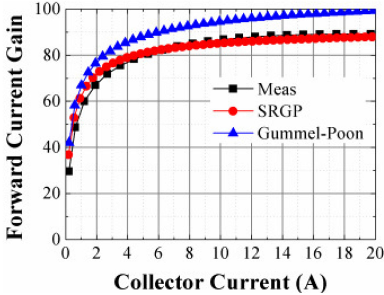

Fig. 6. Comparison of the measured and simulated current gains as a function of the collector current at room temperature.

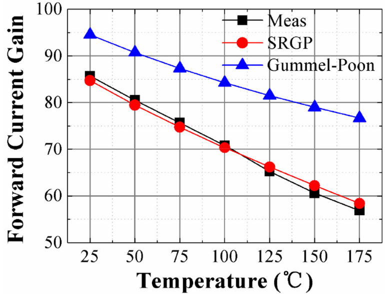

Fig. 7. Comparison of the measured and simulated current gains as a function of temperature.

Gummel–Poon model is approximately 10% larger than the measured current gain, while the SRGP model provides a good match with the measured current gain over a wide collector current range. Fig. 7 shows the SPICE-simulated and measured current gains at different temperatures for $I_B = 105$ mA and $V_{\mathrm{CE}} = 2$ V. The SPICE-simulated current gain using the conventional Gummel–Poon model is much larger than the measured current gain, especially at high temperatures. Figs. 6 and 7 show that the surface recombination effect becomes stronger at larger collector current densities and higher temperatures. An additional diode can effectively model the surface recombination effect that occurred at the SiC/SiO_2 interface.

To validate the SRGP model in the prediction of the dynamic characteristics of the SiC BJT, its switching characteristics were measured using a DPT setup with a clamped inductive load circuit at different dc-link voltages and temperatures. The comparisons of the measured and the SRGP model simulated switching waveforms are shown in Fig. 8, including the collector–emitter voltage V_{CE} and the collector current I_C. A satisfactory agreement between the SPICE-simulated and measured V_{CE} and I_C waveforms during the switching transient is obtained. The oscillations in the measured turn-ON and turn-OFF waveforms of the SiC BJT are mainly induced by the stray inductance in the DPT experimental setup. The stray inductances associated with power devices, dc-link capacitors, and the busbar conductors induce *LC* oscillations during the switching transients of the SiC BJT. In the SPICE simulation circuit, we estimate that the collector and emitter pins of the SiC BJT have a stray inductance of 1.9 and 1.8 nH, respectively. The dc-link capacitors and the busbar conductors have a stray inductance of 0.6 and 3.7 nH, respectively.

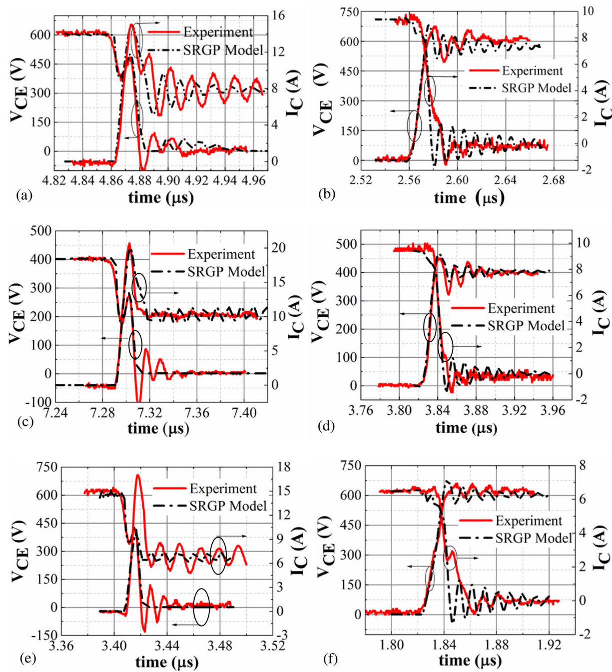

Fig. 8. Zoomed-in views of the measured and SPICE-simulated (a) turn-ON and (b) turn-OFF waveforms at $V_{\mathrm{dc}} = 600$ V, room temperature; (c) turn-ON and (d) turn-OFF waveforms at $V_{\mathrm{dc}} = 400$ V, room temperature; and (e) turn-ON and (f) turn-OFF waveforms at $V_{\mathrm{dc}} = 600$ V, 125 °C.

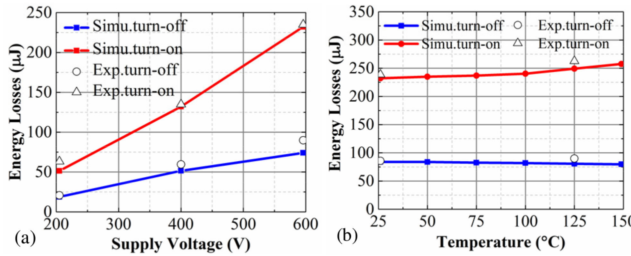

Fig. 9. SPICE-simulated and measured switching energy losses as a function of (a) dc-link voltage and (b) temperature.

In order to further validate the developed SRGP model, the SPICE-simulated and measured switching energy losses of the SiC BJT at different dc-link voltages and temperatures are shown in Fig. 9. The measured switching losses for $V_{\mathrm{CE}} = 200$ V, $V_{\mathrm{CE}} = 400$ V, and $V_{\mathrm{CE}} = 600$ V at a load current of 9 A and at room temperature are calculated and plotted for comparison with SPICE simulation results in Fig. 9(a). In addition, the temperature dependence of the SiC BJT's switching energy losses was investigated by means of SPICE simulation and experimental measurement at a dc-link voltage of 600 V and a load current of 9 A. As shown in Fig. 9(b), both the SPICE simulation and measurement results show that there is little temperature dependence of the SiC BJT's switching energy losses.

B. Implementation in the Proportional Base Driver Design

The relatively high base driver consumption of the SiC BJT in the ON-state hinders its widespread adoption in industrial

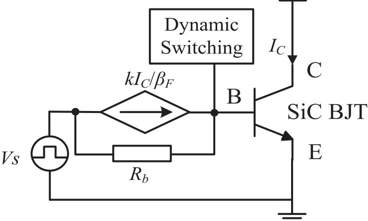

Fig. 10. Schematic of the proportional base driver.

applications. Most traditional base drivers can only provide a relatively large constant base current in the ON-state of the SiC BJT whenever its collector current varies, resulting in a large overdrive current and static power loss in the driver without any benefit to its conduction [6]. A proportional base driver is needed for the SiC BJT to achieve a base driver current that almost proportionally varies with the collector current so that its static power consumption can be greatly reduced when operating in a power electronics system with a variable load, especially at light loads. In this paper, the developed SRGP model is implemented in the design of an SiC BJT based 3.6-kW boost converter with a proportional base driver for circuit simulation and performance assessment.

The schematic of an ideal proportional base driver for the SiC BJT is shown in Fig. 10. It consists of two parallel stages. The dynamic switching stage is used to supply a base current peak during the switching transient [4], while the steady-state stage is used to supply a proportional base current in the ON-state. The ideal steady-state stage of the proportional base driver consists of a current-controlled current source (CCCS) in parallel with a bypass resistor R_b. The bypass resistor R_b is a current-limiting resistor with a large resistance value and is used to ensure a minimum base current when the SiC BJT is turned-ON during the start-up period of the converters. The CCCS is used to provide a base current that can proportionally vary with the collector current of the SiC BJT in the conduction state. Considering an engineering margin (k) for the proportional base driver to ensure that the SiC BJT is fully turned-ON, the optimum base current for the SiC BJT is given by

$$I_{B_\text{Optimum}} = kI_C/\beta_F\,(I_C, T) \tag{28}$$

where the forward common–emitter current gain β_F of the SiC BJT is a function of the collector current I_C and temperature T.

An example to achieve the CCCS in a practical proportional base driver is presented in our study [6]. The schematic circuit of the open-loop boost converter based on the SiC BJT and a proportional base driver is shown in Fig. 11. A Hall current sensor is used to sample the collector current and output a voltage control signal, which is fed to the gate of a signal MOSFET, and to adjust its ON-state resistance. Thus, the base current flowing through the signal MOSFET varies with the collector current. In the proportional base driver, an engineering margin of 1.3 is adopted, and a low voltage supply of 5 V is used to reduce the driver consumption. The duty cycle of the signal is varied in order to imitate the variation of the converter's load current. Fig. 12 shows the measured waveforms of the proportional base

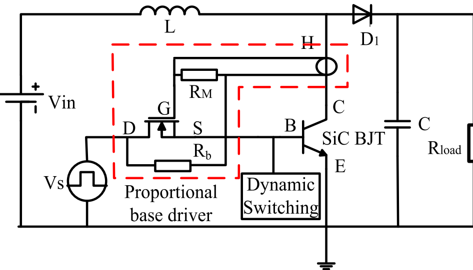

Fig. 11. Designed proportional base driver in an SiC BJT based boost converter.

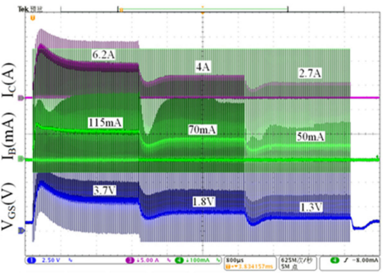

Fig. 12. Measured waveforms of the power converter featuring a proportional base driver technique.

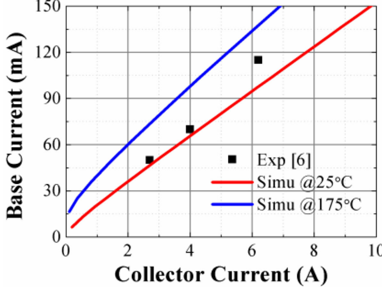

Fig. 13. Comparison of the measured and SPICE-simulated base currents of the proportional base driver.

driver in the SiC BJT based boost converter with three steps of duty cycles at room temperature. The base current and the collector current of the SiC BJT in the steady state at each pulse period are extracted from the measured waveform in order to evaluate the performance of the proportional base driver. When the duty cycle decreases from 0.6 to 0.45 and 0.3 in the boost converter, the collector current of the SiC BJT decreases from 6.2 to 4 and 2.7 A, and the base current decreases from 115 to 70 and 50 mA in the steady state. It means that approximately 70% power consumption of the proportional base driver in the steady-state is reduced under light load conditions.

To evaluate the performance of the designed proportional base driver, we simulated the ideal proportional base driver as shown in Fig. 10 using the developed SRGP model and compared the SPICE-simulated results with the experimental results of the designed proportional base driver in the boost converter. Comparison between the SPICE-simulated base current with 30% engineering safe margin and the measured base current of the proportional base driver is shown in Fig. 13. The red and blue lines represent the simulated base current for the SiC BJT

to ensure that it can operate in the saturation mode at 25 and 175 °C, respectively. The black squares show the measured base currents at different collector currents. Note that when the collector current varies from 6.2 to 2.7 A, the simulated ideal base current is expected to vary from 98 to 46 mA at room temperature if 30% engineering safe margin is taken into consideration, while the measured base current varies from 115 to 50 mA. The small difference between the SPICE-simulated optimum base current and the measured base current indicates that a good design of the proportional base driver with the implementation of the improved SPICE model for the SiC BJT is achieved.

V. Conclusions

The surface recombination effect is a unique phenomenon in the SiC BJT and is one of the key factors inducing the decrease of current gain, especially at large collector currents and high temperatures. According to the SRH recombination theory, the surface recombination effect can be modeled using a diode, and the theoretical emission coefficient of the diode is 2. Considering the practical surface condition, the emission coefficient of the diode modeled for the surface recombination is in the range of 1.5–4. In the conventional Gummel–Poon model, diodes describing the forward base current and the emitter leakage current cannot effectively predict the surface recombination current; hence, the Gummel–Poon model cannot accurately describe the current gain of the SiC BJT over a wide range of collector current and operation temperature.

In this paper, we have proposed an improved SPICE model for the SiC BJT incorporating the surface recombination effect by adding a diode between the external base and emitter terminals. The diode has an emission coefficient of 3.05. Comparison between the experiment and simulation results demonstrates the feasibility of the SRGP model in accurately predicting the SiC BJT's static and dynamic behaviors over a wide range of collector currents and temperatures, and its implementation in the design and evaluation of a proportional base driver in a 3.6-kW boost converter shows its effectiveness to optimize the design of power electronic applications based on SiC BJTs.

References

[1] A. Salemi, H. Elahipanah, K. Jacobs, C.-M. Zetterling, and M. Östling, "15 kV-Class implantation-free 4H-SiC BJTs with record high current gain," *IEEE Electron Device Lett.*, vol. 39, no. 1, pp. 63–66, Jan. 2018.

[2] *Datasheet of GA10JT12-247*, GeneSiC, 2015. [Online]. Available: http://www.genesicsemi.com/images/products_sic/sjt/GA10JT12-247.pdf

[3] H. Miyake, T. Kimoto, and J. Suda, "4H-SiC BJTs with record current gains of 257 on (0001) and 335 on (000–1)," *IEEE Electron Device Lett.*, vol. 32, no. 7, pp. 841–843, Jul. 2011.

[4] J. Rabkowski, G. Tolstoy, D. Peftitsis, and H.-P. Nee, "Low-loss high-performance base-drive unit for SiC BJTs," *IEEE Trans. Power Electron.*, vol. 27, no. 5, pp. 2633–2643, May 2012.

[5] G. Tolstoy, D. Peftitsis, J. Rabkowski, P. R. Palmer, and H.-P. Nee, "A discretized proportional base driver for silicon carbide bipolar junction transistors," *IEEE Trans. Power Electron.*, vol. 29, no. 5, pp. 2408–2417, May 2014.

[6] L. Linyuan, J. Wang, S. Tang, Z. Shuai, X. Yin, and Z. J. Shen, "A new proportional base drive technique for SiC bipolar junction transistors," *IEEE Trans. Power Electron.*, vol. 32, no. 6, pp. 4600–4606, Jun. 2017.

[7] P. A. Ivanov *et al.*, "Factors limiting the current gain in high-voltage 4H-SiC npn-BJTs," *Solid-State Electron.*, vol. 46, pp. 567–572, 2002.

[8] P. A. Ivanov, M. E. Levinshtein, A. K. Agarwal, J. W. Palmourand, and S.-H. Ryu, "Base current gain of power (1800 V, 10 A) 4H-SiC npn-BJTs," *Mater. Sci. Forum*, vol. 457–460, pp. 1145–1148, Jan. 2004.

[9] R. Ghandi *et al.*, "Surface-passivation effects on the performance of 4H-SiC BJTs," *IEEE Trans. Electron Devices*, vol. 58, no. 1, pp. 259–265, Jan. 2011.

[10] C. Sun, Y. Zhang, X. Deng, and B. Zhang, "High current gain 4H-SiC BJT for limiting surface states effect," in *Proc. 12th IEEE Int. Conf. Solid-State Integr. Circuit Technol.*, 2014, pp. 1–3.

[11] J. Zhang, X. Li, P. Alexandrov, L. Fursin, X. Wang, and J. H. Zhao, "Fabrication and characterization of high-current-gain 4H-SiC bipolar junction transistors," *IEEE Trans. Electron Devices*, vol. 55, no. 8, pp. 1899–1906, Aug. 2008.

[12] C. Codreanu, M. Avram, V. Obreja, C. Voitincu, and I. Codreanu, "Interface states and related surface currents in SiC junctions," in *Proc. Int. Semicond. Conf.*, 2003, pp. 297–300.

[13] P. A. Ivanov, M. E. Levinshtein, A. K. Agarwal, S. Krishnaswami, and J. W. Palmour, "Temperature dependence of the current gain in power 4H-SiC NPN BJTs," *IEEE Trans. Electron Devices*, vol. 53, no. 5, pp. 1245–1249, May 2006.

[14] E. Santi, K. Peng, H. A. Mantooth, and J. L. Hudgins, "Modeling of wide-bandgap power semiconductor devices—Part II," *IEEE Trans. Electron Devices*, vol. 62, no. 2, pp. 434–442, Feb. 2015.

[15] S. Balachandran, T. P. Chow, A. Agarwal, W. Tipton, and S. Scozzie, "Gummel–Poon model for 1.8 kV SiC high-voltage bipolar junction transistor," in *Proc. IEEE 35th Annu. Power Electron. Specialists Conf.*, 2004, pp. 2994–2998.

[16] Y. Huang, S. Cheng, W. Zhou, and K. Sheng, "Modeling of a 1200 V 6 A SiC bipolar junction transistor," in *Proc. IEEE Energy Convers. Congr. Expo.*, 2013, pp. 934–939.

[17] D. Johannesson and M. Nawaz, "Development of a simple analytical PSpice model for SiC-based BJT power modules," *IEEE Trans. Power Electron.*, vol. 31, no. 6, pp. 4517–4525, Jun. 2016.

[18] T. Gachovska *et al.*, "Modeling, simulation, and validation of a power SiC BJT," *IEEE Trans. Power Electron.*, vol. 27, no. 10, pp. 4338–4346, Oct. 2012.

[19] F. Sischka, "Gummel–Poon bipolar model: Model description and paremeter extraction," Agilent Technologies GmbH, Munich, Germany.

[20] T. Ohshima, M. Yoshikawa, H. Itoh, Y. Aoki, and I. Nashiyama, "Generation of interface traps and oxide-trapped charge in 6H-SiC metal-oxide-semiconductor transistors by gamma-ray irradiation," *Japanese J. Appl. Phys.*, vol. 37, no. 8, pp. 1002–1004, Aug. 1998.

[21] R. Singh and S. Sundaresan, "Fulfilling the promise of high-temperature operation with silicon carbide devices: Eliminating bulky thermal-management systems with SJTs," *IEEE Power Electron. Mag.*, vol. 2, no. 1, pp. 27–35, Mar. 2015.

[22] *Sentaurus Device User Guide and Sentaurus Workbench User Guide Version K-2015.06*, Synopsys, Mountain View, CA, USA, 2015.

[23] C. H. Henry, R. A. Logan, and F. R. Merritt, "The effect of surface recombination on current in $Al_xGa_{1-x}As$ heterojunctions," *J. Appl. Phys.*, vol. 49, no. 6, pp. 3530–3542, Jun. 1978.

[24] C. T. Sah, "A new semiconductor tetrode—The surface-potential controlled transistor," *Proc. IRE*, vol. 49, no. 11, pp. 1623–1634, 1961.

[25] S. Liang *et al*, "A modified behavior SPICE model for SiC BJT," in *Proc. IEEE Appl. Power Electron. Conf. Expo.*, 2018, pp. 238–243.

Jun Wang (S'06–M'10–SM'15) received the B.S. degree from the Huazhong University of Science and Technology, Wuhan, China, in 2000, the M.S. degree from the Institute of Semiconductors, Chinese Academy of Sciences, Beijing, China, in 2003, the M.E. degree from the University of South Carolina, Columbia, SC, USA, in 2005, and the Ph.D. degree from North Carolina State University, Raleigh, NC, USA, in 2010, all in electrical engineering.

Between 2010 and 2013, he was a Device Design Engineer with Texas Instruments Inc., Bethlehem, PA, USA. In 2014, he was a Professor with the College of Electrical and Information Engineering, Hunan University, Changsha, China. He has authored and coauthored more than 50 journal and conference publications and holds three U.S. patents. His research interests include power semiconductor devices and their applications in power electronic systems.

Since 2017, Dr. Wang has been an Associate Editor for the IEEE Journal of Emerging and Selected Topics in Power Electronics and the CPSS *Transactions on Power Electronics and Applications*.

Shiwei Liang (S'17) received the B.S. degree in electric engineering from the School of Information Science and Engineering, Central South University, Changsha, China, in 2015. He is currently working toward the Ph.D. degree at the College of Electrical and Information Engineering, Hunan University, Changsha, China.

His research interests include SiC power semiconductor devices and their applications in power electronic systems and power integration.

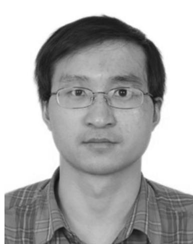

Linfeng Deng received the Ph.D. degree from The University of Hong Kong, Pokfulam, Hong Kong.

He is currently an Assistant Professor with the School of Electrical and Information Engineering, Hunan University, Changsha, China. His research interests include power semiconductor devices and pulse power technology.

Xin Yin received the B.S., M.S., and Ph.D. degrees from the College of Electrical and Information Engineering, Hunan University, Changsha, China, in 1993, 2000, and 2011, respectively, all in electrical engineering.

In 2006, he was an Associate Research with Hunan University. He has participated in the 863 program, NSFC, and several projects supported by the Natural Science Foundation of Hunan Province, China. His research interests include power electronic applications and circuit fault diagnosis.

Dr. Yin was the recipient of the Ministry of Education Science and Technology Progress Award.

Z. John Shen (S'89–M'94–SM'01–F'11) received the B.S. degree from Tsinghua University, Beijing, China, in 1987, and the M.S. and Ph.D. degrees from Rensselaer Polytechnic Institute, Troy, NY, USA, in 1991 and 1994, respectively, all in electrical engineering.

Between 1994 and 1999, he held various positions including the Senior Principal Staff Scientist with Motorola. He was a Faculty Member with the University of Michigan-Dearborn between 1999 and 2004 and with the University of Central Florida between 2004 and 2012. In 2013, he was the Grainger Chair Professor in electrical and power engineering with the Illinois Institute of Technology. He has also held a Courtesy Professorship with Hunan University, Changsha, China, since 2007 and with Zhejiang University, Hangzhou, China, since 2013. His research interests include power electronics, power semiconductor devices and ICs, automotive electronics, renewable and alternative energy systems, and electronics manufacturing.